Electronic Supplementary Information for

Interstitially O-doped $Cd_xZn_{1-x}S$ solid solution derived from chalcogenide molecular clusters for photocatalytic hydrogen evolution

Weijie Yang[a,b], Xiang Wang[b], Zhiqiang Wang[b], Peipei Sun[b], Jiaqi Tang[b], Juan Li[b], Dong-Sheng Li*[,c], and Tao Wu*[,a,b]

[a] *College of Chemistry and Materials Science, Guangdong Provincial Key Laboratory of Functional Supramolecular Coordination Materials and Applications, Jinan University, Guangzhou, Guangdong 510632, China*

[b] *College of Chemistry, Chemical Engineering and Materials Science, Soochow University, Suzhou, Jiangsu 215123, China*

[c] *College of Materials and Chemical Engineering, Hubei Provincial Collaborative Innovation Center for New Energy Microgrid, Key Laboratory of Inorganic Nonmetallic Crystalline and Energy Conversion Materials, China Three Gorges University, Yichang, Hubei 443002, China*

*Corresponding author

E-mail address: lidongsheng1@126.com; wutao@jnu.edu.cn

Characterizations.

The microstructures and morphologies of the photocatalysts obtained above were determined by TEM (HT7700, Hitachi, Japan) and HRTEM (FEI TacnaiG2 F20). Power X-ray (PXRD) diffractometer (D2 PHASER, Cu Kα, Bruker, Germany) was used to characterize the crystal phases of the photocatalysts and their phase purity. The room-temperature electron spin resonance spectra (ESR) were measured on an ESR spectrometer (JES-X320) at 300 K. The UV-Vis diffuse reflection spectra (UV-Vis DRS) were recorded on a SHIMADZU UV-3600 UV-Vis-NIR spectrophotometer by using $BaSO_4$ powder as the reflectance reference. X-ray photoelectron spectroscopy (XPS, Thermo Fisher Scientific ESCLAB 250Xi) was characterized to analyze the binding energies of the elements and valance band (VB) of the photocatalysts. The photoluminescence (PL) were recorded on a HORIBA scientific Fluorolog-3 spectrofluorometer with the corresponding accessories.

Photocatalytic H_2 evolution measurements.

The PHE activity of the title samples was tested in a closed gas circulation system. 20 mg of the sample was dispersed in a 100 mL aqueous solution containing 10 mL sacrificial reagent of triethanolamine. Then, air in reaction solution was removed by vacuuming to 0.5 kPa. During the photocatalytic reaction, the suspension was irradiated under a 300 W xenon lamp (PLS-SXE 300C, Perfectlight) that was positioned 20 cm away from a quartz flask with a focused intensity of 168 mW cm^{-2}, and kept with a continuous magnetic stirring at 5 °C by a flow of cooling water. The evolved gases were analyzed by gas chromatography (GC 7890T, Shanghai, China) equipped with a thermal conductive detector (TCD) and a 5 Å molecular sieve column using N_2 as carrier gas. The PHE recycling tests over the as-prepared photocatalyst were performed as follows. After the first run reaction, the suspension was collected, and the previous steps for another nine cycles were repeated.[1]

Electrochemical and photoelectrochemical measurements

The electrochemical impedance spectroscopy (EIS), Mott-Schottky (M-S), and photocurrent response were tested on CHI 760E in a Na_2SO_4 aqueous solution (0.5 M, pH = 6.8) using a three-electrode system: Ag/AgCl as reference electrode, Pt plate as counter electrode, and photocatalyst-supporting ITO as working electrode. The working electrode was prepared as follows[2]: The ITO conductive glass was sonicated in acetone, water, and ethanol for 30 min, respectively. 10 mg of sample powder and 2 mg of $Mg(NO_3)_2 \cdot 6H_2O$ was dispersed in 20 mL IPA, and continuously stirred for 24 h. Then, the working electrode was fabricated by electro-deposition for 30 min, during which the platinum electrode was used as anode and ITO as the cathode, and constant working voltage was set up to 30 V, while current was zero. Finally, the obtained ITO electrode decorated with sample film on its surface was washed with ethanol to remove residual $Mg(NO_3)_2$ salt.

Results and discussion

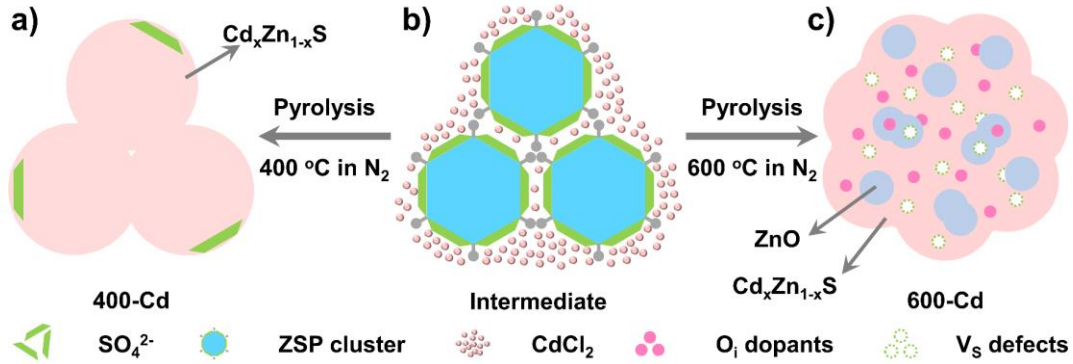

Scheme S1. Proposed structure models of the pyrolyzed products of the mixture of ZSP crystals and $CdCl_2$ salt. a) Product obtained by pyrolyzing the mixture of ZSP crystals and $CdCl_2$ salt at 400 ℃. b) The mixture of ZSP crystals and $CdCl_2$ salt, c) Product obtained by pyrolyzing the mixture of ZSP crystals and $CdCl_2$ salt at 600 ℃.

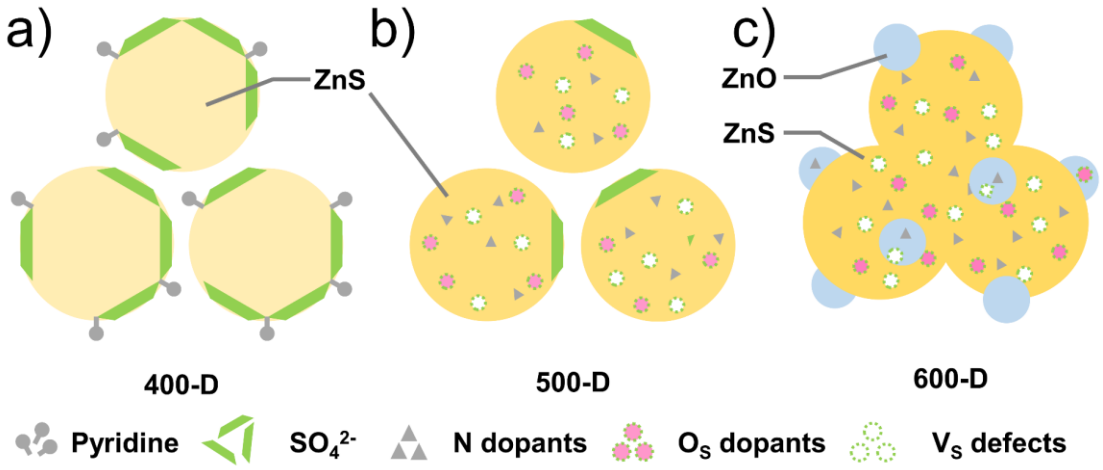

Scheme S2. Proposed structure models of the pyrolyzed products prepared through directly annealing ZSP crystals at 400 ℃ (a), 500 ℃ (b), and 600 ℃ (c).

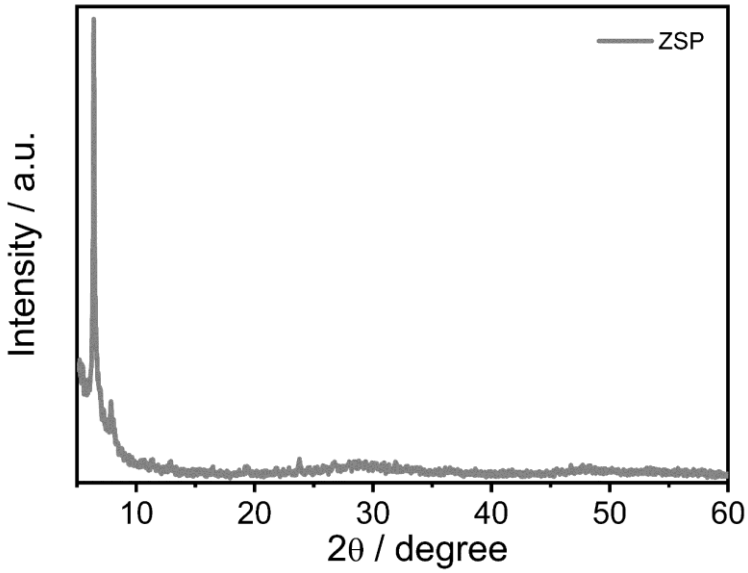

Figure S1. Powder XRD pattern of ZSP microcrystals.

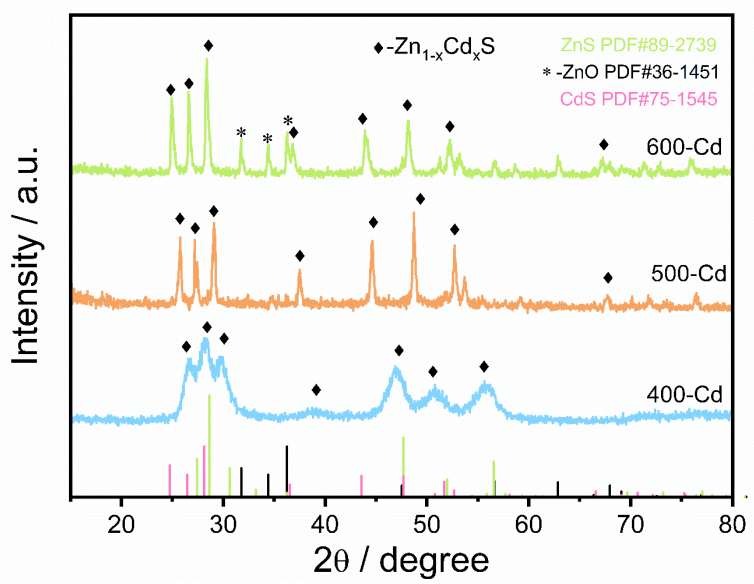

Figure S2. Powder XRD patterns of 400-Cd, 500-Cd, and 600-Cd.

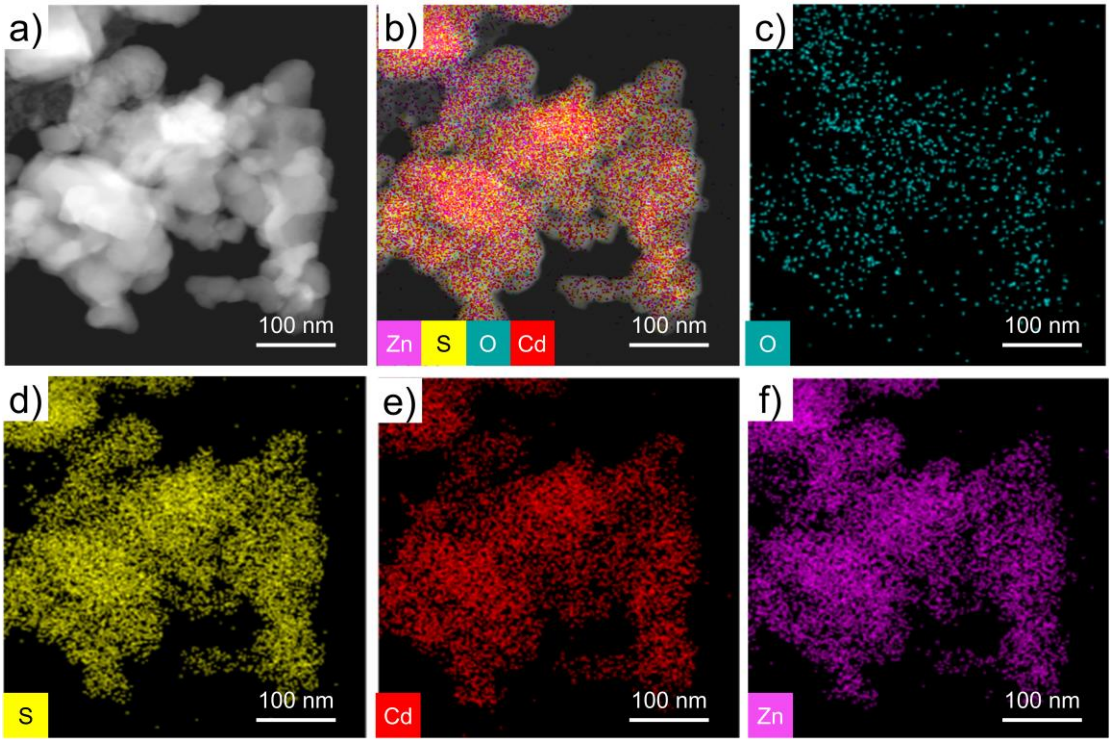

Figure S3. a) HADDF-STEM image of 500-Cd. EDS element mapping images of b) overlay, c) O, d) S, e) Cd and f) Zn for 500-Cd.

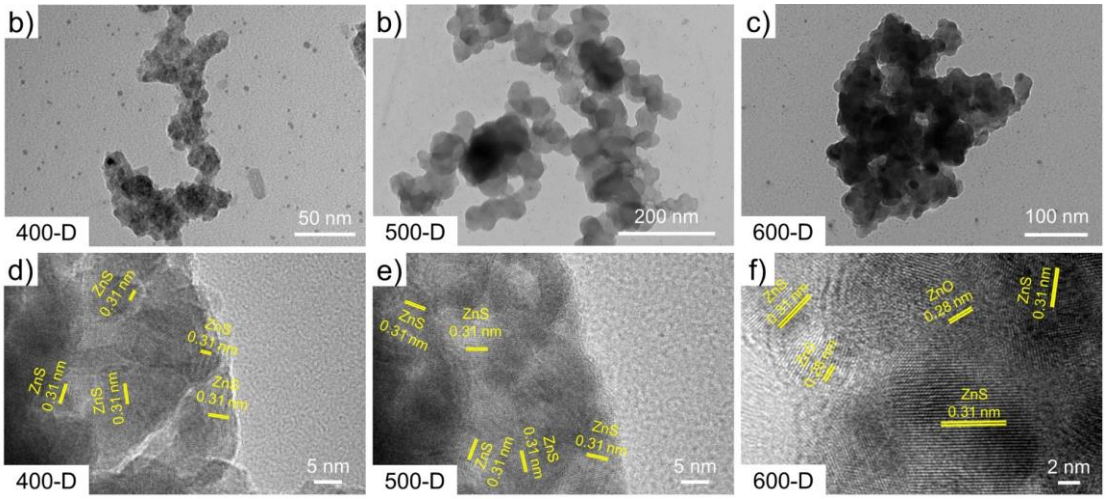

Figure S4. TEM images of a) 400-D, b) 500-D, and c) 600-D. HRTEM images of d) 400-D, e) 500-D, and f) 600-D.

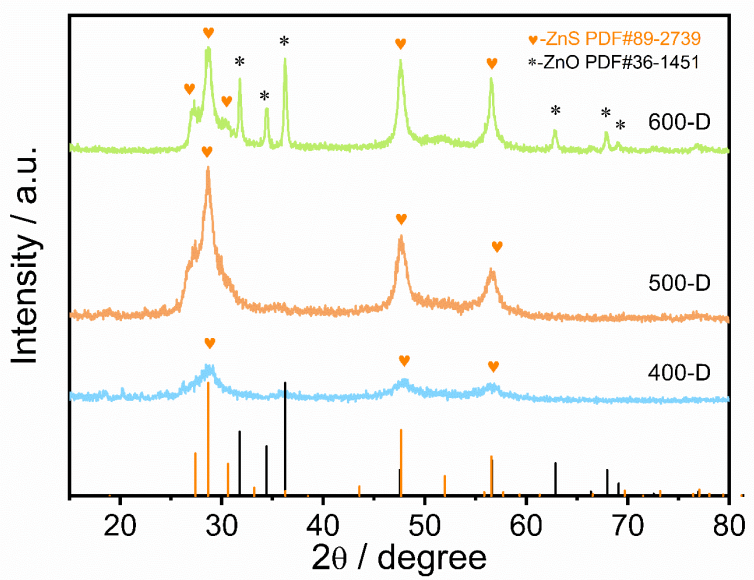

Figure S5. Powder XRD patterns of 400-D, 500-D, and 600-D.

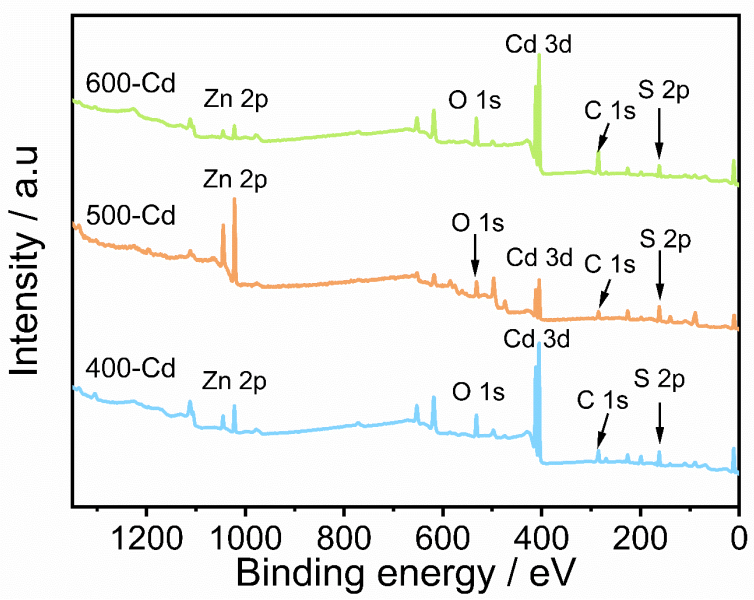

Figure S6. XPS profiles of 400-Cd, 500-Cd, and 600-Cd.

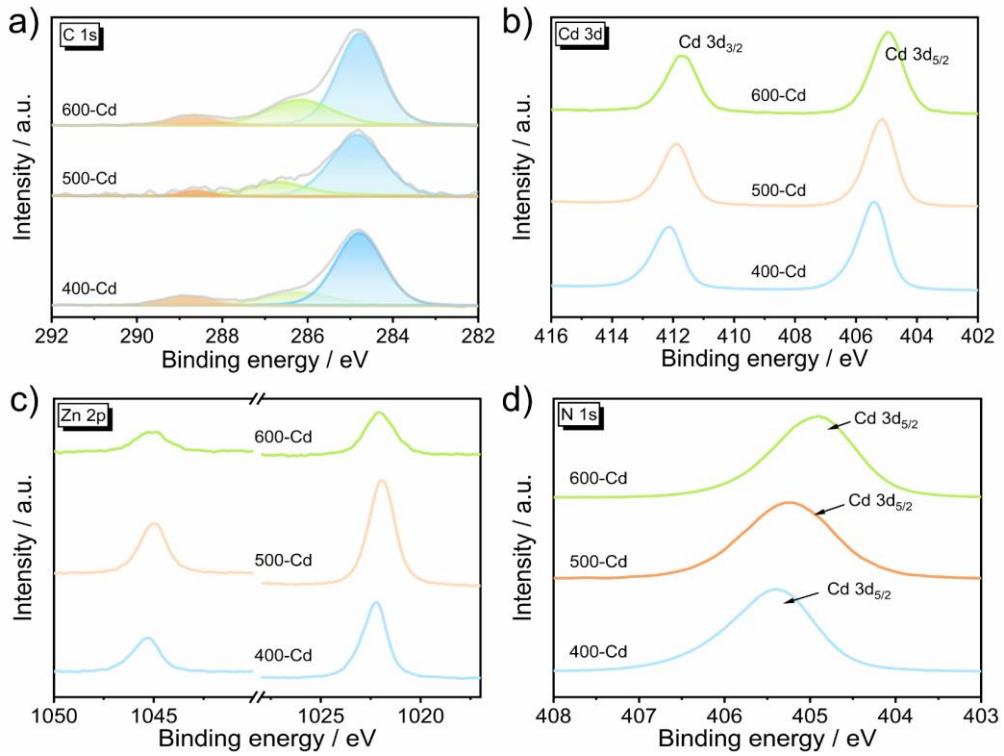

Figure S7. High-resolution XPS profiles of C 1s a), b) Cd 3d, c) Zn 2p, and d) N 1s for 400-Cd, 500-Cd, and 600-Cd.

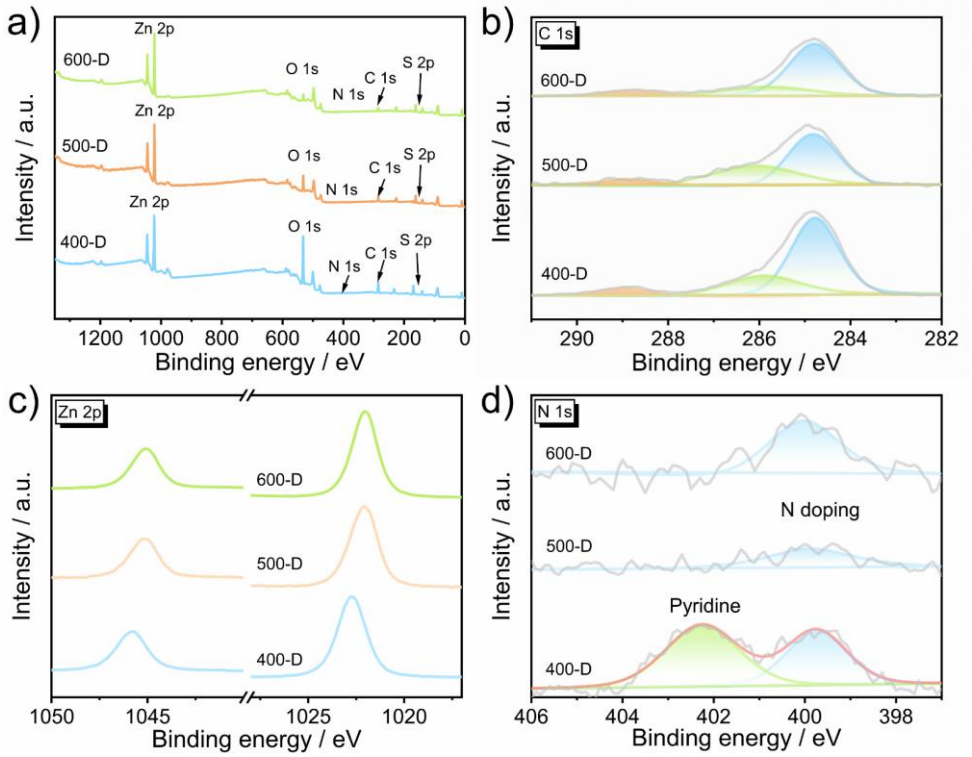

Figure S8. XPS spectra for a survey scan (a) and high-resolution XPS profiles of C 1s (b), Zn 2p (c), and N 1s (d) for 400-D, 500-D, and 600-D.

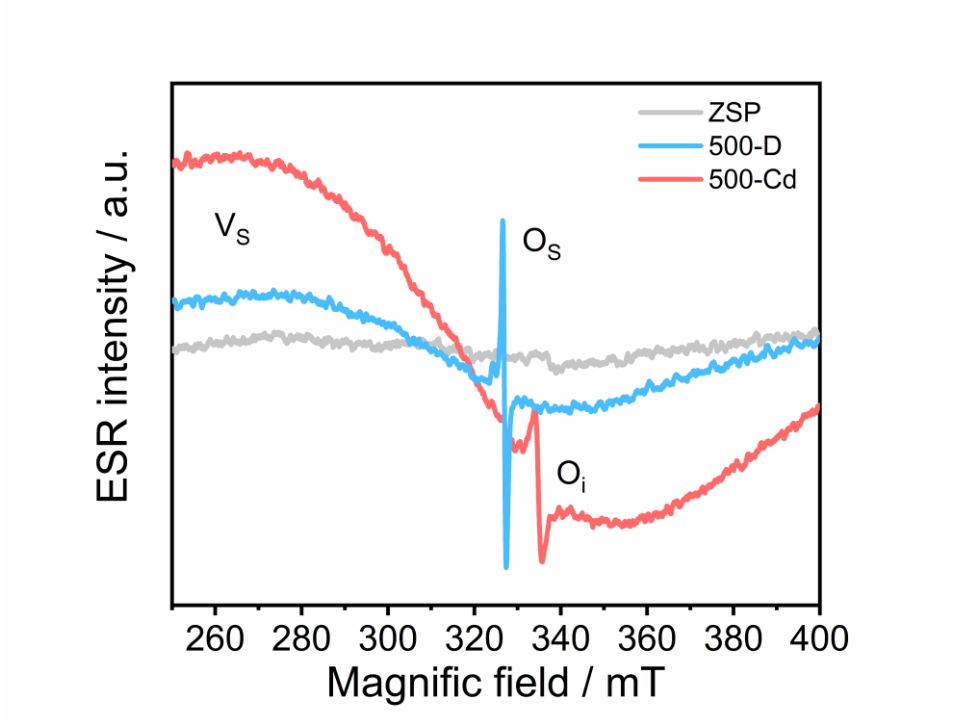

Figure S9. Room-temperature ESR spectra of the as-prepared ZSP microcrystals, 500-D, and 500-Cd.

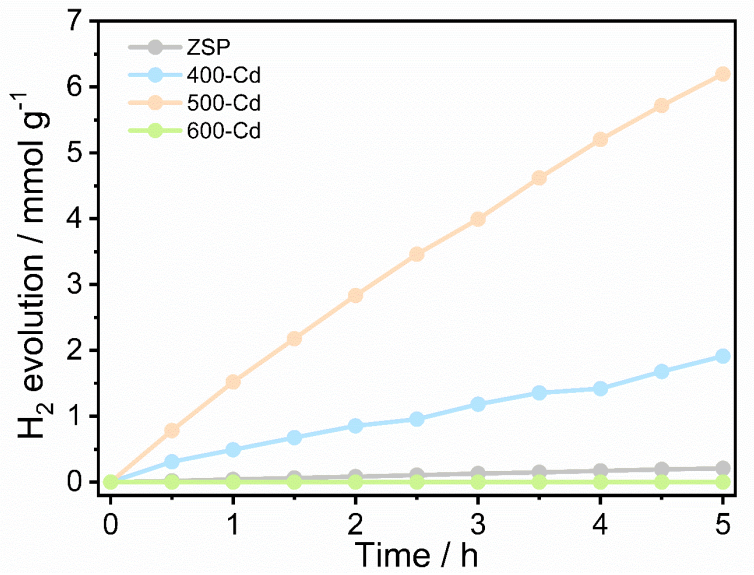

Figure S10. PHE rate of ZSP microcrystals, 400-Cd, 500-Cd, and 600-Cd under 5 h visible-light irradiation.

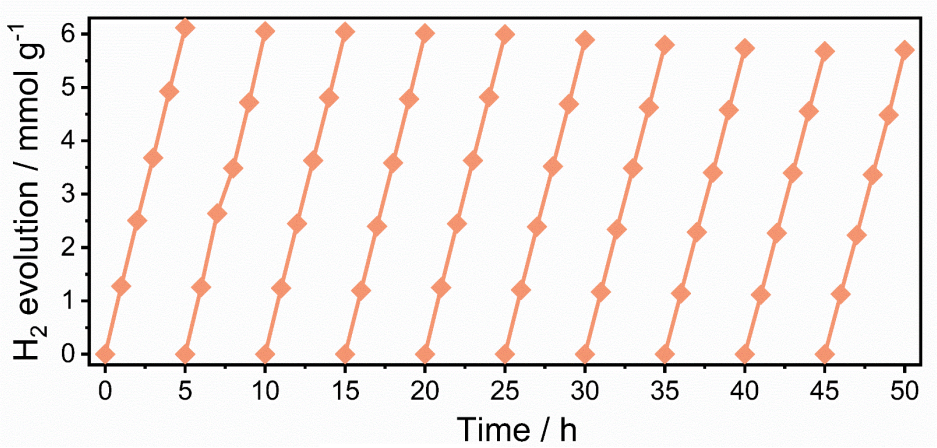

Figure S11. PHE cycling tests of 500-Cd.

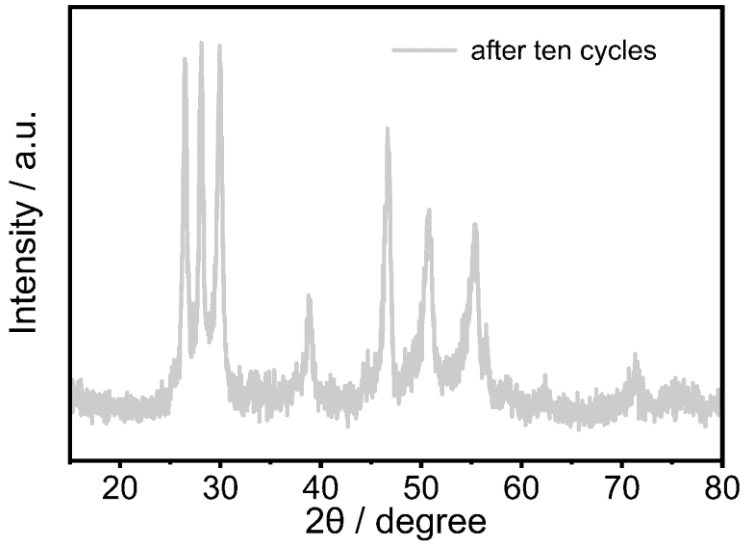

Figure S12. Powder XRD pattern of 500-Cd after PHE cycling test.

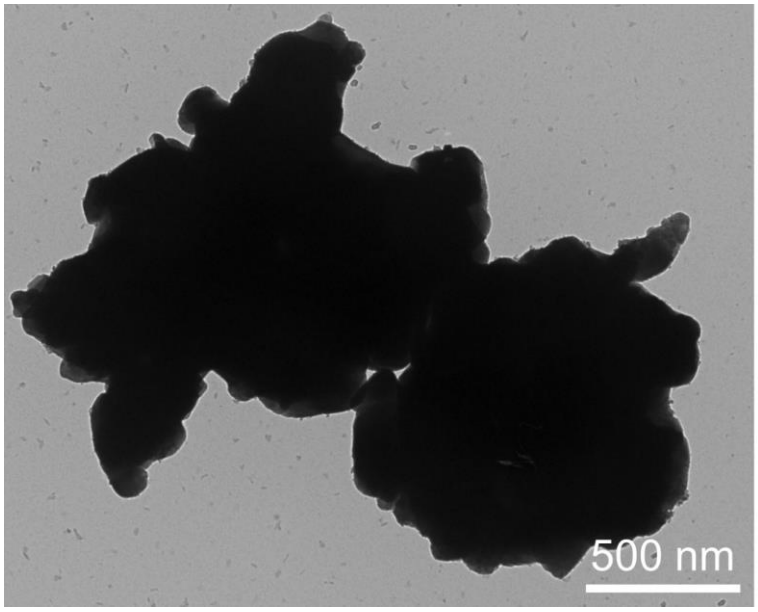

Figure S13. TEM image of 500-Cd after PHE cycling test.

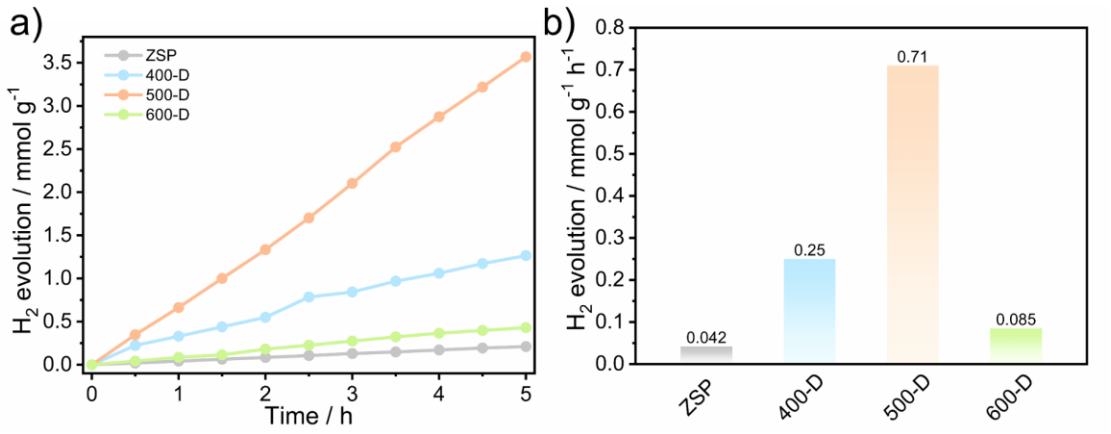

Figure S14. a) Amounts of the generated hydrogen from ZSP microcrystals, 400-D, 500-D, and 600-D under 5 h visible-light irradiation. b) PHE rates of all samples.

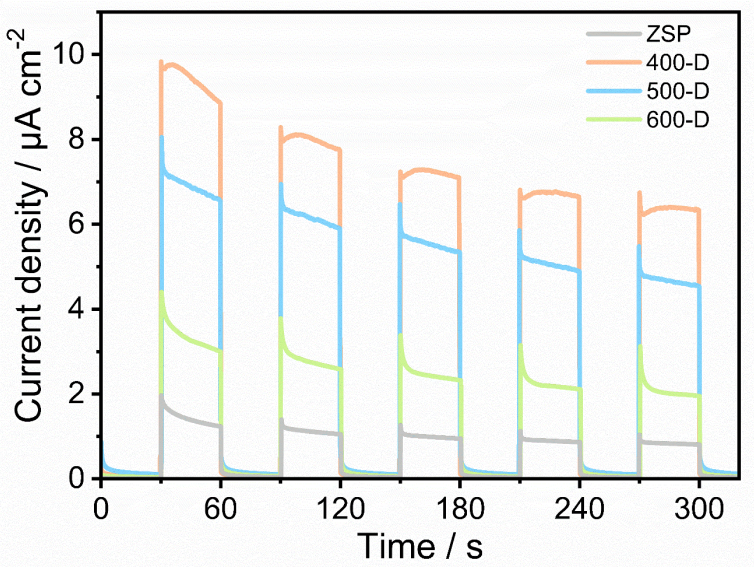

Figure S15. Transient photocurrent response of ZSP, 400-D, 500-D, and 600-D.

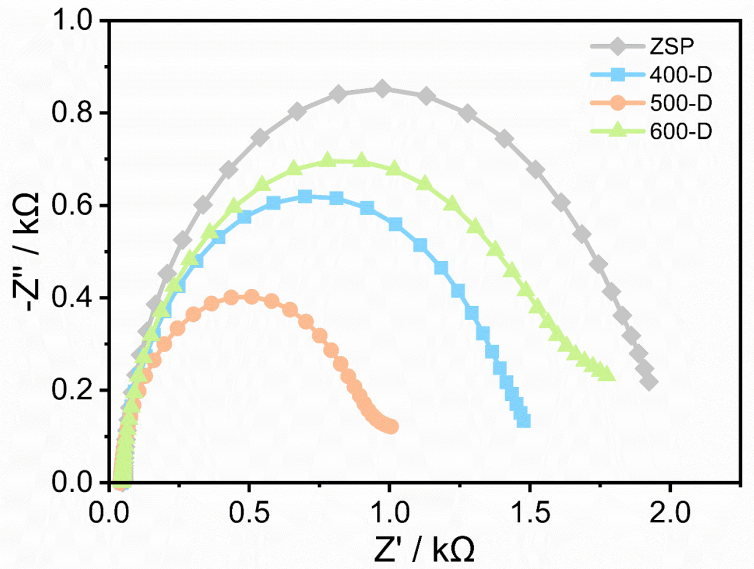

Figure S16. EIS plots of ZSP, 400-D, 500-D, and 600-D.

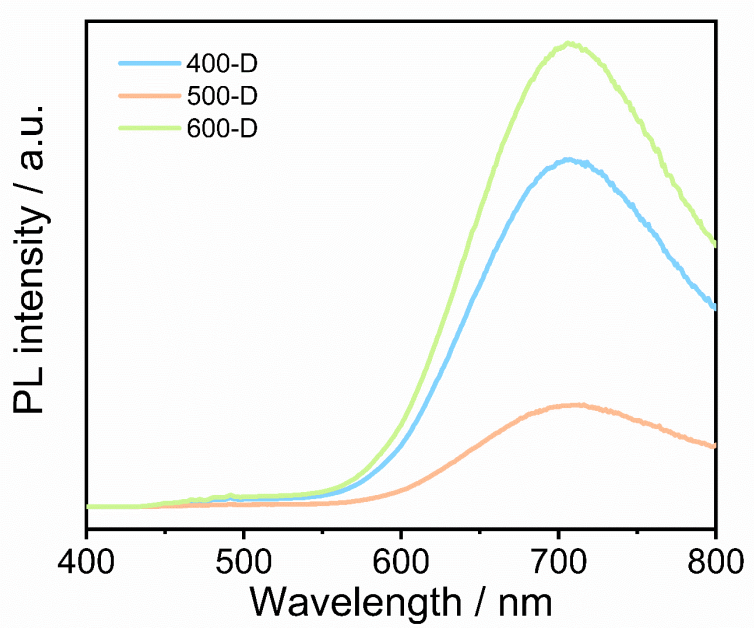

Figure S17. PL spectra of 400-D, 500-D, and 600-D.

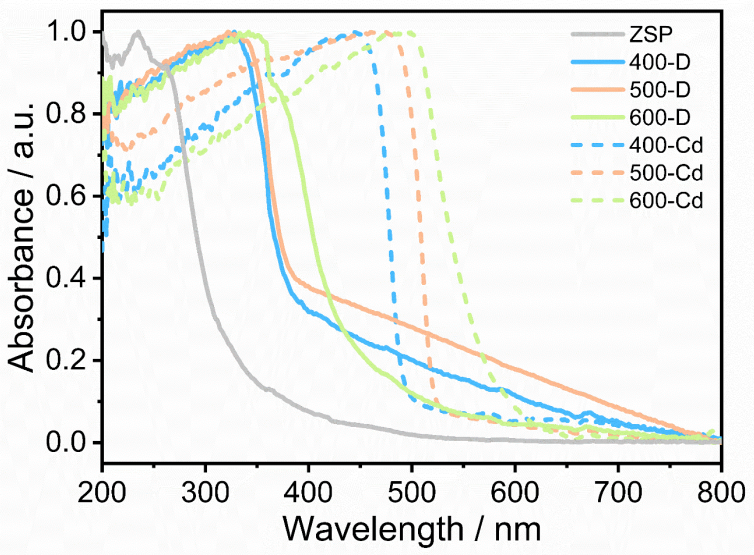

Figure S18. UV-vis diffuse reflectance spectra of all samples.

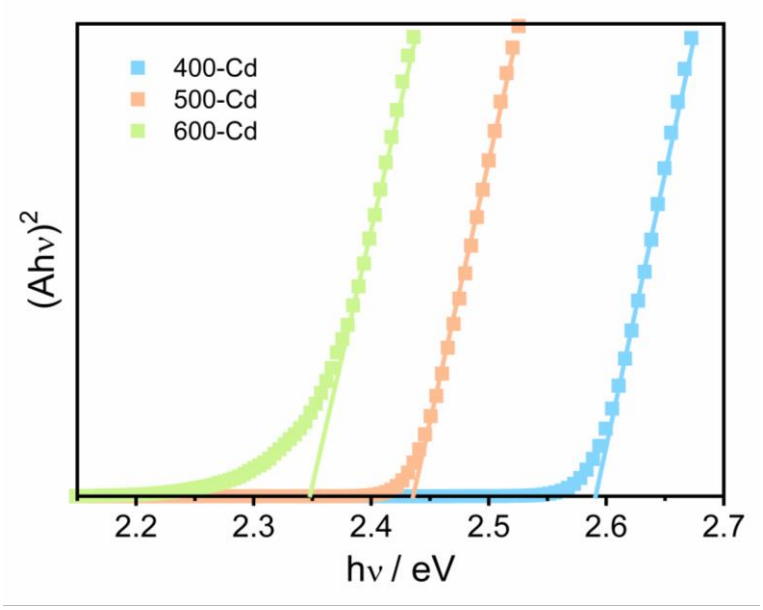

Figure S19. $(\alpha h\nu)^2$ versus $(h\nu)$ plots of 400-Cd, 500-Cd, and 600-Cd.

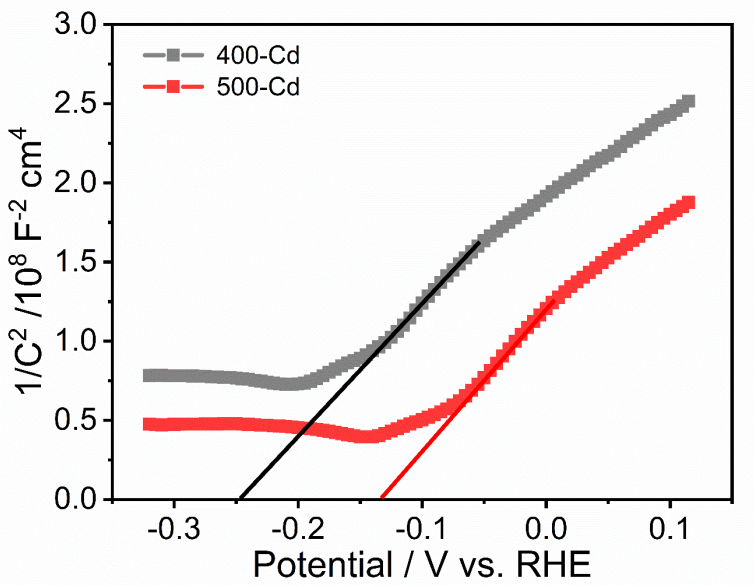

Figure S20. Mott–Schottky plots of 400-Cd and 500-Cd.

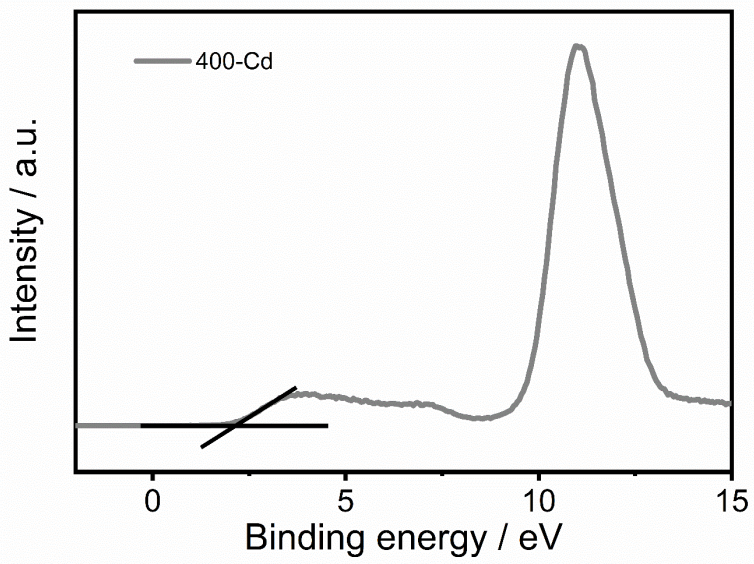

Figure S21. XPS VB plot of 400-Cd.

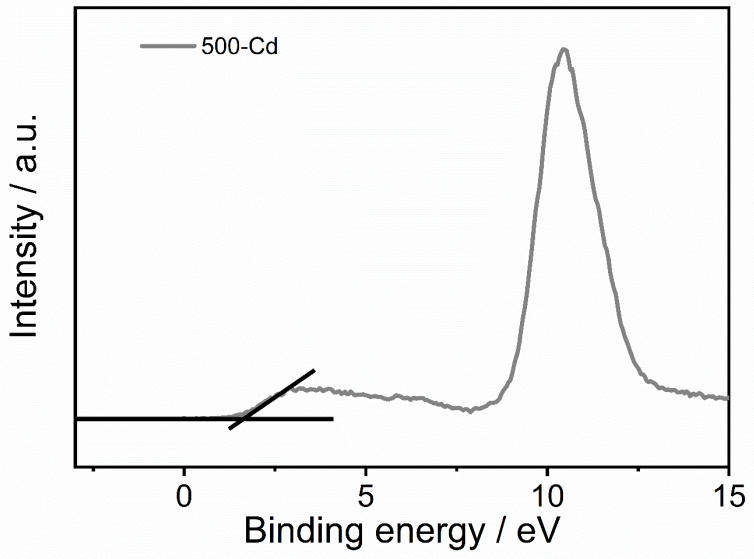

Figure S22. XPS VB plot of 500-Cd.

References

[1] W. Yang, X.-L. Wang, N. Kong, C. Liu, P. Sun, Z. Wang, Y. Ding, H. Lin, D. Li, T. Wu, Minimized external electric field on asymmetric monolayer maximizes charge separation for photocatalysis, *Appl. Catal. B: Environ.* **2021**, 295, 120266.

[2] D. Liu, Y. Liu, P. Huang, C. Zhu, Z. Kang, J. Shu, M. Chen, X. Zhu, J. Guo, L. Zhuge, et al., Highly tunable heterojunctions from multimetallic sulfide nanoparticles and silver nanowires, *Angew. Chem. Int. Ed.* **2018**, 57, 5374-5378.